ELSEVIER

Wave Motion 37 (2003) 183–188

WAVE MOTION

www.elsevier.com/locate/wavemoti

An analytical approach for the fast design of high-power waveguide windows

Ming-Chieh Lin [a,b,*,1], Hao-Ming Chung [a], Alex Burke [c]

[a] *Department of Electrophysics, National Chiao Tung University, Hsinchu 30050, Taiwan, ROC*
[b] *High Temperature Material Section, Material and Electro-Optics Research Division, Chung-Shan Institute of Science and Technology, Tao-Yuan 325, Taiwan, ROC*
[c] *Stanford Linear Accelerator Center, Stanford University, Stanford, CA 94025, USA*

Received 3 January 2002; received in revised form 25 August 2002; accepted 3 September 2002

Abstract

An analytical approach is presented to achieve the fast design of high-power waveguide windows. The analytical calculation is compared with the result of numerical simulation via the finite-element code high frequency structure simulator and the experiments of W-band waveguide windows performed at the Stanford Linear Accelerator Center (SLAC), Stanford University, Stanford, CA. The closed form has been carried out to enhance the accuracy and efficiency, and the exact calculation agrees with the experimental results and the numerical simulation very well.

PACS: 42.25.Bs; 84.40.Az; 84.47.+w

Keywords: Waveguide window; Microwave; Vacuum; Analytical

1. Introduction

In microwave tubes, ceramic microwave windows are generally used to separate the high vacuum of such devices from atmospheric pressure. There are mainly two types of vacuum window for waveguide-output tubes frequently in use. One is a resonance type. The structure is a rectangular waveguide brazed with a dielectric slab whose thickness is $\lambda_g/2$. The value λ_g is the wavelength in the material of the vacuum seal [1–9]. The other is a pillbox type, which is composed of two rectangular waveguides and one cylindrical waveguide brazed with a ceramic disk [10–16]. The schematic views of a rectangular waveguide window and a pillbox window are shown in Fig. 1. The former is a simple structure and can support high-power microwave transmission, but it is very difficult to braze the rectangular ceramic. The latter has the advantage of the reliability of the disk brazing, and has a wide bandwidth. Some of the problems encountered in the use of conventional vacuum-tight microwave output windows including heating and destruction of windows due to high losses, arc-over at high output voltages, poor quality due to temperature

* Corresponding author. Present address: Department of Electrophysics, National Chiao Tung University, Hsinchu 30050, Taiwan, ROC. Tel.: +886-35712121-56142; fax: +886-35725230.
E-mail address: mclin.ep87g@nctu.edu.tw (M.-C. Lin).
[1] Also with Stanford Linear Accelerator Center as a visiting physicist.

0165-2125/02/$ – see front matter
PII: S0165-2125(02)00073-2

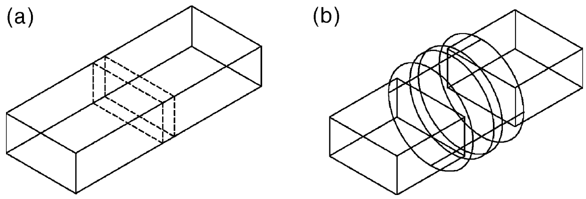

Fig. 1. Schematics of: (a) a rectangular waveguide window and (b) a pillbox window.

limitations of bakeout, and high cost because of expensive geometry. However, there are some basic requirements regarding the properties of a microwave window including low microwave dissipation, low microwave reflection, and a vacuum-tight seal.

For Ku-band or lower frequency, pillbox windows were widely used and easily fabricated. Pillbox windows of millimeter wave tubes become very thin because of extremely high frequency, so that power capacity of the window is limited, manufacturing is difficult and it is prone to air leaks. By comparison, dielectric waveguide windows are thicker and can be easily used for the output of Ka-band millimeter wave tubes or even higher frequency. Recently, it has proven possible to fabricate W-band waveguide windows at the Stanford Linear Accelerator Center (SLAC), Stanford University, Stanford, CA. The experiments were compared with the results of numerical simulation via the finite-difference code GdfidL, giving good agreement [17]. In this paper, we present an analytical approach to achieve the design of high-power waveguide windows with high accuracy and efficiency. The analytical calculation is compared with the results of numerical simulation via the finite-element code, high frequency structure simulator (HFSS), and the experiments.

2. Analytical approach

Let us consider a waveguide with its rectangular cross-section of sides a and b, and the enclosed dielectric slab with thickness, d. The TE mode (H mode) in the rectangular waveguide is characterized by the H_z component of the magnetic field. By definition, this component is never absent in this mode. The z component of the Helmholtz's equation is

$$\left(\frac{\partial^2}{\partial x^2}+\frac{\partial^2}{\partial y^2}+\frac{\partial^2}{\partial z^2}\right)H_z+\omega^2\varepsilon\mu H_z=0. \tag{1}$$

In this case the effect of losses of the medium inside the waveguide is characterized by the complex permittivity ε and permeability μ. The boundary conditions for H_z are

$$\left.\frac{\partial}{\partial x}H_z\right|_{x=0,a}=0, \tag{2}$$

and

$$\left.\frac{\partial}{\partial y}H_z\right|_{y=0,b}=0. \tag{3}$$

Applying the boundary conditions of Eqs. (2) and (3) to the general solution of Eq. (1), which is a constant-coefficient, second-order homogeneous linear differential equation, the following particular solution can be found by means of separation of variables:

$$H_z=H_0\cos\left(\frac{m\pi x}{a}\right)\cos\left(\frac{n\pi y}{b}\right)\exp(\mathrm{j}\omega t-\gamma z). \tag{4}$$

In this equation, H_0 is a constant that is determined by the electromagnetic wave energy propagating inside the waveguide, and m and n are integers. The exponential function is chosen for a particular solution since it represents propagating waves in the z-direction, where γ is the propagation constant of the waveguide to be obtained. In order to obtain γ, Eq. (4) must be substituted into Eq. (1), yielding

$$\gamma = \pm \mathrm{j}\sqrt{\omega^2\varepsilon\mu - \left(\frac{m\pi}{a}\right)^2 - \left(\frac{n\pi}{b}\right)^2} = \pm \mathrm{j}\frac{2\pi}{\lambda}\sqrt{\varepsilon_\mathrm{r}\mu_\mathrm{r} - \left(\frac{\lambda}{\lambda_\mathrm{c}}\right)^2}. \tag{5}$$

In this equation, λ represents the wavelength in free space at the operating angular frequency ω, ε_r and μ_r are the relative dielectric constant and permeability of the medium, respectively, and λ_c is the cutoff wavelength. It then follows that:

$$\lambda_\mathrm{c} = \frac{2}{\sqrt{(m/a)^2 + (n/b)^2}}, \tag{6}$$

where m and n are integers. The magnetic field component H_z can be expressed as

$$H_z = \begin{cases} \mathrm{e}^{-\mathrm{j}k_1 z} + R\,\mathrm{e}^{+\mathrm{j}k_1 z} & \text{for } z \le 0, \\ A\,\mathrm{e}^{-\mathrm{j}k_2 z} + B\,\mathrm{e}^{+\mathrm{j}k_2 z} & \text{for } 0 \le z \le d, \\ S\,\mathrm{e}^{-\mathrm{j}k_3 z} & \text{for } z \ge d, \end{cases} \tag{7}$$

where

$$k_i = \frac{2\pi}{\lambda}\sqrt{\varepsilon_\mathrm{r}\mu_\mathrm{r} - \left(\frac{\lambda}{\lambda_\mathrm{c}}\right)^2} \quad \text{for } i = 1, 2, 3. \tag{8}$$

When considering the losses in the walls for the mode TE_{10}, we should add the term, $-\mathrm{j}\alpha_\mathrm{c}$, to the right-hand side of Eq. (8), where

$$\alpha_\mathrm{c} = \frac{1}{\eta b}\sqrt{\frac{\pi f \mu_\mathrm{c}}{\sigma_\mathrm{c}[1 - (f_\mathrm{c}/f)^2]}}\left[1 + \frac{2b}{a}\left(\frac{f_\mathrm{c}}{f}\right)^2\right]. \tag{9}$$

The coefficients R, A, B, and S in Eq. (7) are determined from the boundary conditions

$$\mu_{\mathrm{r}1}H_z(0^-) = \mu_{\mathrm{r}2}H_z(0^+), \qquad H_z'(0^-) = H_z'(0^+), \qquad \mu_{\mathrm{r}2}H_z(d^-) = \mu_{\mathrm{r}3}H_z(d^+), \qquad H_z'(d^-) = H_z'(d^+). \tag{10}$$

The above equations become

$$\begin{aligned} R &= \frac{(-1+\mathrm{e}^{-2\mathrm{j}k_2 d})k_1k_3\mu_{\mathrm{r}2}^2 - (-1+\mathrm{e}^{-2\mathrm{j}k_2 d})k_2^2\mu_{\mathrm{r}1}^2\mu_{\mathrm{r}3}^2 + (1+\mathrm{e}^{-2\mathrm{j}k_2 d})k_2\mu_{\mathrm{r}2}(k_3\mu_{\mathrm{r}1} - k_1\mu_{\mathrm{r}3})}{(-1+\mathrm{e}^{-2\mathrm{j}k_2 d})k_1k_3\mu_{\mathrm{r}2}^2 + (-1+\mathrm{e}^{-2\mathrm{j}k_2 d})k_2^2\mu_{\mathrm{r}1}^2\mu_{\mathrm{r}3}^2 - (1+\mathrm{e}^{-2\mathrm{j}k_2 d})k_2\mu_{\mathrm{r}2}(k_3\mu_{\mathrm{r}1} + k_1\mu_{\mathrm{r}3})}, \\ A &= \frac{-2k_1\mu_{\mathrm{r}2}(k_3\mu_{\mathrm{r}2} + k_2\mu_{\mathrm{r}3})}{(-1+\mathrm{e}^{-2\mathrm{j}k_2 d})k_1k_3\mu_{\mathrm{r}2}^2 + (-1+\mathrm{e}^{-2\mathrm{j}k_2 d})k_2^2\mu_{\mathrm{r}1}^2\mu_{\mathrm{r}3}^2 - (1+\mathrm{e}^{-2\mathrm{j}k_2 d})k_2\mu_{\mathrm{r}2}(k_3\mu_{\mathrm{r}1} + k_1\mu_{\mathrm{r}3})} \\ B &= \frac{2\mathrm{e}^{-2\mathrm{j}k_2 d}(k_3\mu_{\mathrm{r}2} - k_2\mu_{\mathrm{r}3})}{(-1+\mathrm{e}^{-2\mathrm{j}k_2 d})k_1k_3\mu_{\mathrm{r}2}^2 + (-1+\mathrm{e}^{-2\mathrm{j}k_2 d})k_2^2\mu_{\mathrm{r}1}^2\mu_{\mathrm{r}3}^2 - (1+\mathrm{e}^{-2\mathrm{j}k_2 d})k_2\mu_{\mathrm{r}2}(k_3\mu_{\mathrm{r}1} + k_1\mu_{\mathrm{r}3})}, \\ S &= \frac{-4\,\mathrm{e}^{-2\mathrm{j}(k_2-k_3)d}k_1k_3\mu_{\mathrm{r}2}\mu_{\mathrm{r}3}}{(-1+\mathrm{e}^{-2\mathrm{j}k_2 d})k_1k_3\mu_{\mathrm{r}2}^2 + (-1+\mathrm{e}^{-2\mathrm{j}k_2 d})k_2^2\mu_{\mathrm{r}1}^2\mu_{\mathrm{r}3}^2 - (1+\mathrm{e}^{-2\mathrm{j}k_2 d})k_2\mu_{\mathrm{r}2}(k_3\mu_{\mathrm{r}1} + k_1\mu_{\mathrm{r}3})}. \end{aligned} \tag{11}$$

If $k_2 d = p\pi$, where p is an integer, then we obtain

$$R = \frac{k_2\mu_{\mathrm{r}2}(k_3\mu_{\mathrm{r}1} - k_1\mu_{\mathrm{r}3})}{k_2\mu_{\mathrm{r}2}(k_3\mu_{\mathrm{r}1} + k_1\mu_{\mathrm{r}3})}, \qquad S = \frac{2\mathrm{e}^{-\mathrm{j}(k_2-k_3)d}k_1k_3\mu_{\mathrm{r}2}\mu_{\mathrm{r}3}}{2k_2\mu_{\mathrm{r}2}(k_3\mu_{\mathrm{r}1} + k_1\mu_{\mathrm{r}3})}. \tag{12}$$

There is an optimum transmission when $k_1/\mu_{r1} = k_3/\mu_{r3}$. For $p = 2$, we have

$$d = \frac{\lambda}{\sqrt{\varepsilon_{r2}\mu_{r2} - (\lambda/\lambda_c)^2}}. \tag{13}$$

Eq. (13) is used to determine the thickness of the ceramic window, which is a full guide wavelength for the SLAC experiments. Eq. (11) is used to yield the S-parameters as functions of frequency.

3. Results and discussion

For a good match, the window should be a multiple of half the dielectric guide wavelength. A $p = 2$ or "$1 - \lambda$" window design as a compromise between bandwidth and ease of assembly is selected for the experiments performed at SLAC. Several W-band waveguide windows have been fabricated and tested. The dielectric consists of WesCo AL-995 alumina ceramic of dimensions 2.49 mm × 1.22 mm × 1.09 mm, and it is brazed into an oxygen-free high-conductivity (OFE) copper WR10 (2.54 mm × 1.27 mm) rectangular waveguide with the length of 76.2 mm. The dielectric constant ε_{r2} is treated as a fit parameter and is inferred to be 9.485 at 91.4 GHz.

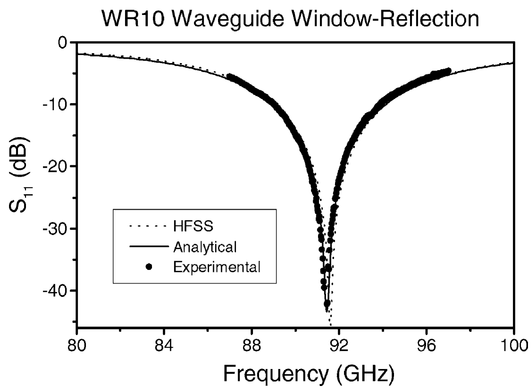

Fig. 2. Plot of the measured reflection of the W-band waveguide window, S_{11} (dB), and the fit of the analytical calculation compared with the numerical simulation via the HFSS code.

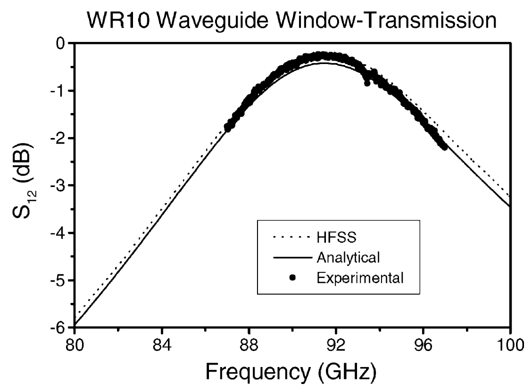

Fig. 3. Plot of the measured transmission of the W-band waveguide window, S_{12} (dB), and the fit of the analytical calculation compared with the numerical simulation via the HFSS code.

Experimental measurements of the reflection parameter, S_{11} (dB) $= 10\log R^2$, for the W-band waveguide window, as a function of frequency, seen in Fig. 2, were fit with the analytical calculation. Also seen in Fig. 2 is the result of numerical simulation via the finite-element code HFSS, giving good agreement. The center frequency is 91.4 GHz and the bandwidth for the transmission of 99%, i.e., S_{11} below -20 dB, is 1.55 GHz or 1.7%, from 90.625 to 92.175 GHz. Fig. 3 shows the results of the corresponding transmission, S_{12} (dB) $= 10\log S^2$. Both the analytical calculation and the numerical simulation via the HFSS code were performed on a workstation equipped with two 1.7 GHz CPUs and 2 GB RAM. It took nearly 3 hr to get the results from the HFSS code, but only about 3 s for the analytical calculation.

4. Conclusion

In conclusion, we have presented an analytical approach to achieve the fast design of high-power waveguide windows. The analytical solution is compared with the result of numerical simulation via the finite-element code HFSS and the experiments performed at the SLAC, Stanford University, Stanford, CA. The closed form of the *S*-parameters has been carried out to enhance the accuracy and efficiency of the window design, and the calculation is in excellent agreement with the experimental results and with the numerical simulation.

Acknowledgements

The authors want to acknowledge the support and encouragement of George Caryotakis, Glenn Scheitrum, and Daryl W. Sprehn, and the computer assistance of Cecilio Vazquez and Rafael J. Gomez, Stanford Linear Accelerator Center (SLAC), Stanford University, Stanford, CA.

References

[1] H.K. Jenny, F.E. Vaccaro, A step-type, broadband, X-band ceramic waveguide window, IRE Trans. Electron Devices 3 (1) (1956) 30–32.
[2] R. Walls, S. Bernabei, H.E. Evans, Fabrication of phased array microwave waveguides windows, in: Proceedings of the13th Symposium of IEEE on Fusion Engineering, vol. 1, 1989, pp. 205–206.
[3] L. Shunkang, A fast computational technique for RF window in millimeter wave tubes, Int. J. Infrared Millimeter Waves 15 (5) (1994) 856–860.
[4] M. Pisharody, P. Barnes, E. Chojnacki, R. Durand, T. Hays, R. Kaplan, J. Kirchgessner, J. Reilly, H. Padamsee, J. Sears, High power window tests on a 500 MHz planar waveguide window for the CESR upgrade, in: Proceedings of the 1995 Part. Accel. Conference, vol. 3, 1995, pp. 1720–1722.
[5] Y. Otake, S. Tokumoto, H. Mizuno, Design and high-power test of a TE11-mode X-band RF window with taper transitions, in: Proceedings of the 1995 Part. Accel. Conference, vol. 3, 1995, pp. 1590–1592.
[6] E. Chojnacki, T. Hays, J. Kirchgessner, H. Padamsee, M. Cole, T. Schultheiss, Design of a high average power waveguide window, in: Proceedings of the 1997 Part. Accel. Conference, vol. 3, 1997, pp. 3177–3179.
[7] H.Z. De, Direct sealing of millimeter-wave transmission window, in: Proceedings of the 1998 International Conference on Microwave and Millimeter Wave Technology, 1998, pp. 718–721.
[8] T. Schultheiss, V. Christina, M. Cole, J. Rathke, T. Elliott, V. Nguyen, L. Phillips, J. Preble, A high thermal conductivity waveguide window for use in a free electron laser, in: Proceedings of the 1999 Part. Accel. Conference, New York, vol. 2, 1999, pp. 780–782.
[9] V. Nguyen, H.L. Phillips, J. Preble, Development of a 50 KW CW L-band rectangular window for Jefferson Lab FEL Cryomodule, in: Proceedings of the 1999 Part. Accel. Conference, New York, vol. 2, 1999, pp. 1459–1461.
[10] J.H. Jasberg, J.V. Lebacqz, High power microwave windows, in: Proceedings of the Fifth International Congress on Microwave Tubes, September 14–18, Paris, 1964, pp. 246–250.
[11] C. Pappas, A.J. Prommer, A.J. Smith, High average power microwave windows, in: Proceedings of the Fifth International Congress on Microwave Tubes, September 14–18, Paris, 1964, pp. 254–255.
[12] D.H. Preist, R.C. Talcott, R. Hayes, Improvement to high power microwave windows, in: Proceedings of the Fifth International Congress on Microwave Tubes, September 14–18, Paris, 1964, pp. 266–271.

[13] H. Arai, N. Goto, Y. Ikeda, T. Imai, An analysis of a vacuum window for lower hybrid heating, IEEE Trans. Plasma Sci. 14 (6) (1986) 947–954.
[14] H. Nakatsuka, N. Yoshida, I. Fukai, Three-dimensional analysis of a vacuum window connected to waveguide, IEEE Trans. Plasma Sci. 16 (4) (1988) 416–422.
[15] Y. Ikeda, T. Imai, K. Sakamoto, Discharge at the pillbox window for an LHRF launcher, IEEE Trans. Plasma Sci. 17 (3) (1989) 534–540.
[16] S. Michizono, Y. Saito, S. Yamaguchi, S. Anami, Dielectric materials for use as output window in high power klystrons, IEEE Trans. Electr. Insul. 28 (4) (1993) 692–699.
[17] M.E. Hill, R.S. Callin, D.H. Whittum, High-power vacuum window in WR10, IEEE Trans. Microwave Theory Technol. 49 (5) (2001) 994–995.